Angular Resolution Improvement of Infrared Phased-Array Antennas

Brian A. Slovick, *Student Member, IEEE*, Jeffrey A. Bean, *Member, IEEE*, and Glenn D. Boreman, *Senior Member, IEEE*

***Abstract*—Measured and simulated angular response patterns at 10.6 μm demonstrate considerable improvement in angular resolution with a four-element phased-array antenna versus that of a two-element array. Due to propagation loss in the transmission line that connects the antenna elements, further resolution improvement is minimal with a six-element phased array. Additional measurements of a two-element array with increased metal thickness indicate that further improvement in angular resolution is possible by reducing propagation loss in the transmission line. With the combination of additional antenna elements and reduced propagation loss, substantial improvement in the angular resolution of off-broadside performance is also observed. All devices use a metal–oxide–metal tunnel diode as the detector element.**

***Index Terms*—Dipole antennas, directional antennas, infrared detectors, phased arrays.**

I. Introduction

INFRARED (IR) dipole antenna-coupled metal–oxide–metal (MOM) tunnel diodes provide a unique detection mechanism that allows for determination of the polarization and wavelength of an optical field [1]. By integrating the MOM diode with a phased-array antenna, the angle of incidence and degree of coherence of received IR radiation can also be determined [2], [3]. Selection of a preferred reception angle is achieved with a pair of dipole antennas coupled to a MOM diode through a coplanar-strip (CPS) transmission line [4]–[6]. The direction of maximum angular response is altered by varying the position of the MOM diode along the transmission line that connects the antennas [7].

Although large angles of incidence are accessible with a two-element array, the width of the angular response pattern, or angular resolution, is limited by the antenna separation, which is bounded from above by the emergence of grating lobes [8]. By increasing the number of antenna elements while keeping the separation fixed, the effective antenna aperture can be made larger, and the angular resolution higher, without introducing grating lobes into the angular response. Further improvement in angular resolution can be realized by reducing propagation loss in the CPS waveguide [4], [6]. One possibility is to increase the confinement of electric fields between the coplanar strips by increasing the metal thickness. This has the effect of increasing the power density of the CPS mode by decreasing the cross-sectional area of the mode.

Manuscript received December 16, 2010; revised January 24, 2011; accepted February 08, 2011. Date of publication February 14, 2011; date of current version March 14, 2011.

The authors are with the Center for Research and Education in Optics and Lasers (CREOL), The College of Optics and Photonics, University of Central Florida, Orlando, FL 32816 USA (e-mail: bslovick@creol.ucf.edu; jbean@creol.ucf.edu; boreman@creol.ucf.edu).

Color versions of one or more of the figures in this letter are available online at http://ieeexplore.ieee.org.

Digital Object Identifier 10.1109/LAWP.2011.2114632

II. Background

The oxide layer in a metal–oxide–metal diode represents a classical potential energy barrier for electrons. If the two metals have different work functions, an electric field is present in the oxide without external applied bias. When coupled to a half-wavelength dipole antenna, infrared radiation introduces an additional time-harmonic bias at the diode. When this optically induced bias has the same polarity as the work function difference, the electric field in the oxide layer is enhanced, and the probability for electrons to tunnel through the oxide barrier increases [9]. The tunneling of electrons through the insulator layer generates more current than expected from Ohm's law, and thus to a nonlinear I–V characteristic. The dc or rectified component of the current is the time average of the current when expanded in a Taylor series with respect to voltage [10]

$$I_{\mathrm{r}} = \frac{1}{4}\left.\frac{d^2 I}{dV^2}\right|_{V=V_{\mathrm{b}}} V_0^2 \tag{1}$$

where V_0 is amplitude of the optical voltage and V_{b} is the bias voltage. The proportionality constant is determined by solving the Schrödinger equation for the relevant potential barrier geometry. For a simple trapezoidal shape, the proportionality constant depends on the metal work functions, the oxide thickness, and the electrical resistance of the barrier [11]. Equation (1) is a semiclassical expression that relates the rectified current, a quantum mechanical quantity, to the classical optical power. As such, (1) allows one to calculate a quantity proportional to the rectified current using a classical electromagnetic solver [7].

Fig. 1 contains electron micrographs of the phased arrays under consideration. The MOM diode is centered in the array, and the dipole antennas are periodically spaced by a distance d. We have not included data on the situation where a dipole is placed at the center of the array. The angular pattern in that case is almost completely determined by the center antenna since there is no propagation loss for that element. Infrared radiation incident on the array induces an electric field with a maximum at the center of the dipoles. A fraction of this energy is transferred to the CPS in the form of confined radiation and electrical currents. The electric field that remains after propagation along the CPS generates a time-dependent bias voltage across the MOM diode. An additional bias voltage is supplied by the short metallic strip that connects the CPS to the MOM diode.

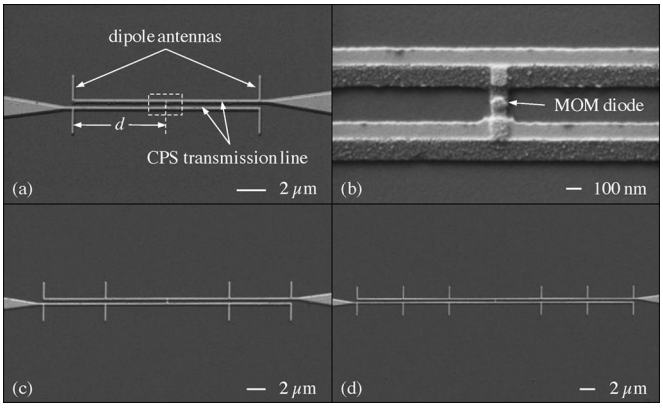

Fig. 1. Electron micrographs of (a) two-, (c) four-, and (d) six-element infrared phased-array antennas. SEM in (b) shows the MOM diode and CPS transmission line.

Such a term is necessary because the axis of the strip is along the direction of the incident polarization. The metal strip can be modeled as a detuned dipole antenna with a real coupling efficiency $\kappa < 1$. The tapered dc lead lines do not contribute significantly to the measured response because they are perpendicular to the incident polarization and large compared to the dipole antennas. This is verified by modeling and by measurement of a negligible cross-polarized response.

For a thin oxide layer, the optical voltage V_i supplied to the MOM diode is approximately proportional to the amplitude of the electric field at the junction. Its value depends on the electromagnetic boundary conditions imposed by the surrounding dielectric or conductive environment, which in general depend on the angle of incidence θ. If the diode is fabricated on a planar substrate, $V_i(\theta)$ is proportional to the magnitude of the electric-field amplitude transmission coefficient for the interface [12]. When the diode is integrated with a phased-array antenna, additional voltage sources are present with relative phase determined by the interference of CPS antenna currents at the location of the diode. Therefore, the array contribution depends on the angle of incidence, the element spacing d, number of antenna elements N, and the CPS attenuation constant α. With these considerations, the total bias voltage induced across the diode can be written as

$$V_0(\theta) = V_i(\theta) \times \left[\kappa + \sum_{m=1}^{N/2} \cos\left(m\frac{2\pi}{\lambda_0} d\sin\theta\right)\exp(-m\alpha d/2)\right] \quad (2)$$

where λ_0 is the free-space wavelength and the summation accounts for the contribution of additional antenna elements. The applied voltage takes the conventional form of the product of the element pattern with an array factor [13].

From (2), one finds that the width of the angular response pattern can be narrowed in several ways. In the simplest case, no array is present (a single antenna), and the angular response pattern is determined by $V_i(\theta)$. In this case, one can tailor the angular response of the device by manipulating the substrate configuration [14]. When the phased array is included, the magnitude of its contribution is determined by the number of antenna elements and the CPS propagation loss. The purpose of this investigation is to determine how these mechanisms influence the angular response pattern of infrared phased-array antennas.

When additional antenna elements are included in the array, the effective aperture of the antenna increases. Because of diffraction, a wider aperture produces a narrower angular response. This effect is apparent in (2) since the contribution to the voltage from the outer elements is a modulation with increased angular frequency. However, if the propagation loss is large, the IR currents generated by the outer elements are attenuated when they reach the diode. As a result, the modulation term in (2) is diminished, and the angular response resembles the single element pattern $V_i(\theta)$, which for typical substrate configurations is quite broad [14]. If the propagation loss is negligible, the modulation term is comparable in magnitude to κ, leading to a modulation that decreases rapidly with the angle of incidence, and thus to a narrowed angular response pattern.

III. Design and Fabrication

Electromagnetic simulations are performed in Ansoft High Frequency Structure Simulator (HFSS), a commercial electromagnetic finite element solver. The antenna structure is modeled in detail within HFSS, including the overlapping metals from the two-angle evaporation process as well as the intermediate aluminum-oxide layer. The optical properties of the materials, including refractive index and film thickness, are measured using a J. A. Woollam Infrared Variable-Angle Spectroscopic Ellipsometer (IR-VASE) and incorporated into the electromagnetic models to increase the accuracy of the simulations [15].

From (1), a quantity proportional to the rectified current is computed as the power dissipated in the aluminum-oxide volume. The power dissipated represents the amount of electromagnetic energy that is converted to thermal energy. To simulate the F/8 measurement setup, the antenna is excited in HFSS with a Gaussian beam of waist $w_0 = 115$ μm with wavelength 10.6 μm (28.3 THz). A radiation pattern is generated by computing the power dissipated in the oxide volume for each angle of incidence [7].

Primary design considerations include the substrate configuration, antenna length and spacing, CPS separation, and metal thickness. From (2), the total voltage supplied to the MOM diode is given by the product of the single-element pattern $V_i(\theta)$ with an array factor. In order to produce the widest single-element pattern, the devices are fabricated on a quarter-wavelength dielectric layer above a ground plane [14]. The dielectric is a 1.7-μm layer of benzocyclobutene (BCB), a low-loss insulator $(k = 0.015)$ with a refractive index of $n = 1.55$ in 10.6 μm infrared region. The use of a low-index substrate also reduces inhomogeneities in the dielectric environment, leading to increased symmetry in the near fields and reduced propagation loss in the CPS [6].

The antenna length and CPS separation are chosen to optimize power transfer from free-space radiation to guided modes in the CPS [7], [16]. This is accomplished in HFSS by terminating a CPS transmission line with a MOM diode and monitoring the response while varying the CPS separation and antenna length. From a parametric analysis in HFSS, the optimal antenna length and CPS separation are 4 μm and 470 nm center

to center, respectively. This antenna length also corresponds to one half-wavelength at a BCB–air interface for a free-space wavelength of 10.6 μm [17]. The dipole antenna and CPS widths are 100 and 260 nm, respectively.

The separation of the antenna elements determines both the width and location of the maxima in the angular response pattern. Although the angular resolution improves as the antenna separation increases, the secondary maxima increase in magnitude as they shift toward small angles [8]. Therefore, the antenna separation is chosen to simultaneously optimize the angular resolution while minimizing the magnitude of the sidelobes. From a parametric analysis in HFSS, the optimal separation is $d = 6.45$ μm, consistent with past research for two-element arrays [7].

Fabrication of antenna-coupled MOM diodes is accomplished with a single-electron-beam lithography exposure and electron beam evaporation of two metals with an intermediate oxidation step [1], [18]. By performing the evaporation at two opposing angles, a small overlap area, typically 75×75 nm^2, is generated where the two metals coincide beneath a suspended bridge of undercut electron beam resist [Fig. 1(b)]. For the metal layers, aluminum and platinum are chosen for their large work function difference and high conductivity in the IR [19]. The thickness of each metal layer is either 45 nm (hereafter nm/layer) or 25 nm/layer. Prior to the Pt layer deposition, oxygen is released into the vacuum chamber at 50 mtorr to allow the Al elements to form an oxide layer 1–2 nm thick. The complete antenna structure, including the lead lines, bond pads, antenna-coupled CPS, and diode, are fabricated without breaking vacuum in the evaporation chamber.

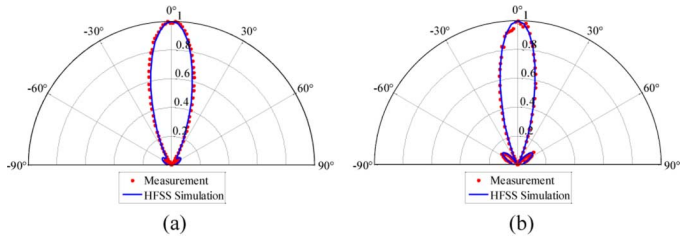

Fig. 2. Measured and simulated angular response patterns in the H-plane of a two-element phased array with a metal thickness of (a) 25 and (b) 45 nm/layer.

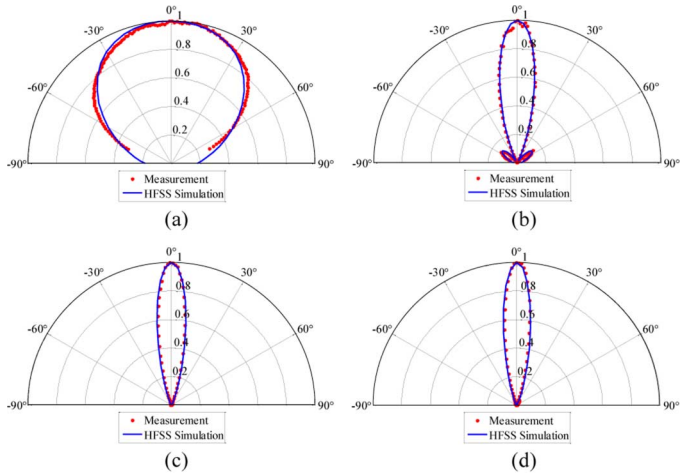

Fig. 3. Measured and simulated angular response patterns in the H-plane of (a) a single dipole antenna and (b) two-, (c) four-, and (d) six-element phased-array antennas.

IV. Results

Infrared measurements are conducted with a 10.6-μm CO_2 laser. The laser is mechanically chopped at 1.5 kHz and focused at F/8 onto the phased-array antenna, which is connected to a five-axis goniometer [20]. The rectified current from the diode is passed through an external current preamplifier and monitored with a lock-in amplifier that is referenced to the frequency of the mechanical chopper. Temporal fluctuations in the laser power are removed by dividing the rectified current by the reference power. During an H-plane radiation pattern measurement, the polarization of the CO_2 laser is oriented along the dipole antennas, while the goniometer is rotated in the plane perpendicular to the axis of the dipoles. Five measurements are averaged at each angle of incidence from -70° to 70°. All measurements are conducted without applied bias and with a laser irradiance of approximately 10 W cm^{-2}, well within the region where the MOM diode acts as square law detector [19]. For all devices, the response to radiation polarized perpendicular to the dipoles is nearly equal to the Johnson noise, which indicates that the thermal and dc lead-line contributions are negligible.

To investigate the influence of propagation loss on the width of the angular response pattern, two-element phased arrays are fabricated with metal thicknesses of 25 and 45 nm/layer. Fig. 2 shows the measured and simulated angular response patterns with the incident polarization along the dipole antennas (H-plane). Measured and simulated data are normalized to their maximum values and plotted linear in power to emphasize features of the main lobe in the angular response. For the antenna with increased metal thickness, the full width at half-maximum (FWHM) is reduced from 35° to 27°. Such an improvement in angular resolution can be attributed to a reduction in propagation loss as a result of increased confinement of the electric fields between the coplanar strips. As the CPS propagation loss increases, the contribution from the array diminishes, and the radiation pattern increasingly resembles the single-element pattern. Additional simulations verify that no further beam narrowing is observed for metal thicknesses beyond 45 nm or CPS widths greater than 260 nm.

To demonstrate the effect of additional antenna elements on the angular resolution, one-, two-, four-, and six-element phased-arrays are fabricated on a fixed BCB substrate with 45 nm/layer. Fig. 3 shows the measured and simulated angular response patterns in the H-plane. As the number of antenna elements increases, the angular resolution improves from 120° FWHM for a single dipole to 27° for a two-element array, 21° for a four-element array, and 19.5° for a six-element array. No further beam narrowing is observed beyond the six-element array due to propagation loss in the CPS. From diffraction theory, the FWHM of an N-element array of equal-amplitude point sources varies as $\lambda_0/(2Nd)$, where d is defined in Fig. 1 [13]. Although the measured FWHM for a two-element array is quite close to the expected value, propagation loss leads to a significant amplitude taper for the four- and six-element

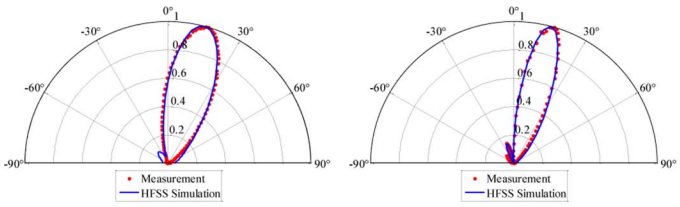

Fig. 4. Measured and simulated angular response patterns in the H-plane of a (a) two-element array with 25 nm/layer and 0.9-μm diode shift and (b) four-element array with 45 nm/layer and 1.5-μm diode shift.

arrays, with less beam narrowing than would be expected for equal-amplitude arrays, but lower sidelobe levels as well. Simulations indicate that the E-plane response for all arrays closely resembles the E-plane response for a single dipole at a BCB–air interface.

We now proceed to compare the off-broadside angular performance of multiple-element phased arrays with 45 nm/layer to current state-of-the-art two-element devices with 25 nm/layer. To do so, we fabricate a four-element array with 45 nm/layer and the diode shifted by 1.5 μm and a two-element array with 25 nm/layer and the diode shifted by 0.9 μm. The diode shifts are determined from a parametric analysis in HFSS to achieve the same reception angle of 15° for both antennas [7]. A four-element phased array is chosen for its simplicity of design and nearly equivalent performance to the six-element array. Fig. 4 shows the measured and simulated H-plane angular response patterns. Substantial beam narrowing is observed for the four-element array with thicker metal. The FWHM is reduced from 38° to 21°. Here, the narrowing of the radiation pattern is due to both the additional antenna elements as well as reduced propagation loss in the CPS from the increased metal thickness.

V. Conclusion

The angular resolution of a two-dipole phased-array antenna is determined by the separation of the antenna elements. Although improvement in angular resolution is possible by increasing the antenna separation, the emergence of grating lobes into the angular response prohibits the array from operating as a high-resolution, unidirectional receiver. By increasing the number of antenna elements while keeping the separation fixed, the effective antenna aperture can be made larger, and the angular resolution narrower, without introducing grating lobes into the angular response. Measured and simulated angular response patterns at 10.6 μm demonstrate considerable improvement with a four-element array and moderate improvement with a six-element array, the latter attributed to propagation loss in the CPS transmission line that connects the antenna elements. Additional measurements of a two-element array with increased metal thickness indicate that further improvement in angular resolution is possible by reducing propagation loss in the transmission line. In addition, substantial improvement in off-broadside angular resolution is observed with a four-element array, thus motivating the use of multiple-element IR phased arrays for rudimentary lensless-imaging applications.

References

[1] J. Bean, B. Tiwari, G. Szakmany, G. Bernstein, P. Fay, and W. Porod, "Antenna length and polarization response of antenna-coupled MOM diode infrared detectors," *Infrared Phys. Technol.*, vol. 53, pp. 182–185, 2010.

[2] C. Middlebrook, P. Krenz, B. Lail, and G. Boreman, "Infrared phased-array antenna," *Microw. Opt. Technol. Lett.*, vol. 50, no. 4, pp. 719–723, 2008.

[3] C. Middlebrook, M. Roggemann, G. Boreman, N. Subotic, K. Cooper, W. Buller, W. Yang, and J. Alda, "Measurement of the mutual coherence function of an incoherent infrared field with a gold nano-wire dipole antenna array," *Int. J. Infrared Millim. Waves*, vol. 29, pp. 179–187, 2008.

[4] T. A. Mandviwala, B. A. Lail, and G. D. Boreman, "Infrared-frequency coplanar striplines: Design, fabrication, and measurements," *Microw. Opt. Technol. Lett.*, vol. 47, pp. 17–20, 2005.

[5] J. Wen, S. Romanov, and U. Peschel, "Excitation of plasmonic gap waveguides by nanoantennas," *Opt. Exp.*, vol. 17, pp. 5925–5932, 2009.

[6] P. Krenz, R. Olmon, B. Lail, M. Raschke, and G. Boreman, "Near-field measurement of infrared coplanar strip transmission line attenuation and propagation constants," *Opt. Exp.*, vol. 18, no. 21, pp. 21678–21686, 2010.

[7] B. Slovick, J. Bean, P. Krenz, and G. Boreman, "Directional control of infrared antenna-coupled tunnel diodes," *Opt. Exp.*, vol. 18, no. 20, pp. 20960–20967, 2010.

[8] W. H. Von Aulock, "Properties of phased arrays," *Proc. IRE*, vol. 48, no. 10, pp. 1715–1727, Oct. 1960.

[9] M. Heiblum, S. Wang, J. R. Whinnery, and T. K. Gustafson, "Characteristics of integrated MOM junctions at dc and optical frequencies," *IEEE J. Quantum Electron.*, vol. QE-14, no. 3, pp. 159–169, Mar. 1978.

[10] I. Codreanu, F. González, and G. Boreman, "Detection mechanisms in microstrip antenna-coupled infrared detectors," *Infrared Phys. Technol.*, vol. 44, pp. 155–163, 2003.

[11] A. Sanchez, C. F. Davis, Jr., K. C. Liu, and A. Javan, "The MOM tunneling diode: Theoretical estimate of its performance at microwave and infrared frequencies," *J. Appl. Phys.*, vol. 49, no. 10, pp. 5270–5277, 1978.

[12] D. B. Rutledge and M. S. Muha, "Imaging antenna arrays," *IEEE Trans. Antennas Propag.*, vol. AP-30, no. 4, pp. 535–540, Jul. 1982.

[13] C. A. Balanis, *Antenna Theory: Analysis and Design*, 3rd ed. Hoboken, NJ: Wiley, 2005.

[14] J. Bean, B. Slovick, and G. Boreman, "Influence of substrate configuration on the angular response pattern of infrared antennas," *Opt. Exp.*, vol. 18, no. 21, pp. 21705–21713, 2010.

[15] J. Ginn, B. Lail, D. Shelton, J. Tharp, W. Folks, and G. Boreman, "Characterizing infrared frequency selective surfaces on dispersive media," *ACES J.*, vol. 22, no. 1, pp. 184–188, 2007.

[16] J.-S. Huang, T. Feichtner, P. Biagioni, and B. Hecht, "Impedance matching and emissions properties of nanoantennas in an optical nanocircuit," *Nano Lett.*, vol. 9, no. 5, pp. 1897–1902, 2009.

[17] C. Fumeaux, M. Gritz, I. Codreanu, W. Schaich, F. González, and G. Boreman, "Measurement of resonant lengths of infrared dipole antennas," *Infrared Phys. Technol.*, vol. 41, pp. 271–281, 2000.

[18] J. A. Bean, B. Tiwari, G. H. Bernstein, P. Fay, and W. Porod, "Thermal infrared detection using dipole antenna-coupled metal-oxide-metal diodes," *J. Vac. Sci. Technol. B*, vol. 27, no. 1, pp. 11–14, 2009.

[19] J. Bean, A. Weeks, and G. Boreman, "Performance optimization of antenna-coupled Al/AlOX/Pt tunnel diode infrared detectors," *IEEE J. Quantum Electron.*, vol. 47, no. 1, pp. 126–135, Jan. 2011.

[20] P. Krenz, B. Slovick, J. Bean, and G. Boreman, "Alignment procedures for radiation pattern measurements of antenna-coupled infrared detectors," *Opt. Eng.*, vol. 49, no. 4, pp. 033607-1–033607-5, 2010.